Applied Mathematical Modelling 81 (2020) 487–505

Contents lists available at ScienceDirect

Applied Mathematical Modelling

journal homepage: www.elsevier.com/locate/apm

Analysis of wave propagation in functionally graded piezoelectric composite plates reinforced with graphene platelets

Chunlei Li, Qiang Han*, Zhan Wang, Xin Wu

School of Civil Engineering and Transportation, South China University of Technology, Guangzhou, Guangdong Province 510640, P.R. China

ARTICLE INFO

Article history:
Received 20 August 2019
Revised 17 December 2019
Accepted 9 January 2020
Available online 16 January 2020

Keywords:
Wave propagation
Graphene reinforcements
Piezoelectric composite plate
Semi-analytical approach
Isogeometric analysis

ABSTRACT

This paper presents a semi-analytical approach to investigate wave propagation characteristics in functionally graded graphene reinforced piezoelectric composite plates. Three patterns of graphene platelets (GPLs) describe the layer-wise variation of material properties in the thickness direction. Based on the Reissner-Mindlin plate theory and the isogeometric analysis, elastodynamic wave equation for the piezoelectric composite plate is derived by Hamilton's principle and parameterized with the non-uniform rational B-splines (NURBS). The equation is transformed into a second-order polynomial eigenvalue problem with regard to wave dispersion. Then, the semi-analytical approach is validated by comparing with the existing results and the convergence on computing dispersion behaviors is also demonstrated. The effects of various distributions, volume fraction, size parameters and piezoelectricity of GPLs as well as different geometry parameters of the composite plate on dispersion characteristics are discussed in detail. The results show great potential of graphene reinforcements in design of smart composite structures and application for structural health monitoring.

1. Introduction

Composite materials are widely used in aerospace, civil, automotive and other engineering fields due to superior properties [1–3], which usually consist of the reinforcement phase and the matrix [4]. The former is the discontinuous, stiffer and stronger while the latter is continuous, less stiff, weaker and lightweight. Carbon-based nanofillers are often used as the reinforcements in composites owing to their extraordinary physical characteristics [5–7]. As the representative candidate, GPLs can provide the bonding strength with the matrix and the high capacity of load transferring in virtue of the high specific surface area [8]. It is proved that GPLs are superior to the other of Carbon-based nanofillers [9]. By blending a small amount of graphene sheets, the Young's modulus of the poly composites can be enhanced significantly [10]. Up to now, graphene-reinforced nanocomposites have atracted considerable academic attention on the analysis of vibration, buckling and impact behaviors [11–14].

Besides, owing to the wide applications in structural health monitoring, electronics devices, piezoelectric materials and composite structures have been focused by many scholars, especially for excitation and propagation of wave signals in structures [15]. Considering the shear effect and rotary inertia, wave propagation in piezoelectric coupled cylinder was analyzed

* Corresponding author.
E-mail address: emqhan@scut.edu.cn (Q. Han).

https://doi.org/10.1016/j.apm.2020.01.016
0307-904X/

by Liew et al. [16]. Wang et al. [17] studied theoretically wave propagation characteristics in piezoelectric cylindrical laminated shells and the effects of large deformation, stacking sequences and piezoelectric layers on wave dispersion were also discussed. Yu et al. [18] used the Legendre orthogonal polynomial series expansion approach to determine wave characteristics hollow cylinders composed of functionally graded piezoelectric materials, based on the linear three-dimensional piezoelectricity. Recently, Wu et al. [19] reported wave characteristics in piezoelectric laminated fiber-reinforced composite cylindrical shells with the transverse shear effects and rotary inertia. Then, they analyzed wave propagation in piezoelectric cylindrical shell reinforced with carbon nanotubes based on the Mori-Tanaka micromechanical model and the shear deformation shell theory [20].

Moreover, the previous experiments have indicated that piezoelectric and dielectric properties of the PVDF can be improved and enhanced by graphene reinforcements as well as mechanical properties [21–23]. With the advantages inherited from PVDF, that is low density, physical flexibility, high piezoelectric constants, high sensitivity, quick response and so on, graphene reinforced piezoelectric nanocomposites can be applied in design and fabrication of different electronic components including audio transducers of microphone and loudspeaker, electromechanical transducers of blood pressure gauge, tactile sensors and wearable electronics, ultrasonic transducers in nondestructive testing (NDT) and structural health monitoring (SHM). Especially in coupled piezoelectric composite structures, signals transmit by the form of elastic waves, which benefit the understanding and application of information transmission in electronic devices and defect detection in NDT. Meanwhile, the instructions have also been shown at the end of the revised manuscript. However, to the authors's knowledge, there are few literatures focused on wave propagation of the piezoelectric composite structures reinforced with GPLs. Only Zhang et al. [24,25] reported vibration and buckling analyses of functionally graded graphene reinforced piezoelectric composite plates with the von Karman nonlinear theory and the differential quadrature method. It was found that the GPLs are beneficial to achieve improved smart composite structures. Therefore, the functionally graded graphene reinforced piezoelectric composite plates are considered here for wave propagation.

For analyzing wave propagation, the above literatures mainly concentrate on analytical solutions based on the theories of plates or shells [26], and in terms of numerical calculation, there have been several numerical methods developed in the past decades on basis of the finite element method (FEM) [27–30]. Although these methods can be performed by using the FEM codes, they may suffer from high cost and low accuracy in structural analysis. To overcome the shortcoming, an potential numerical approach, namely isogeometric analysis [31] is employed here, which utilizes the NURBS to exactly describe the geometry and physical fields of waveguides without additional process of mesh generation. The inherent discretization error of the classical FEM can be efficiently avoided due to the high smoothness and continuity [32].

According to the literature survey, the IGA has been successfully integrated with the plate theories for analyzing vibration and buckling problems. Based on the classical plate theory, Shojaee et al. [33] developed a NURBS-based finite element method to consider free vibration and buckling behaviors of laminated composite plates, and then, the same method was used to study static bending, vibration, buckling and flutter of functionally graded plates [34]. Besides, Yu et al. [35] proposed a simple first order locking-free deformation formulation to consider static and dynamic performances of functionally graded plates in the framework of IGA. The isogeometric formulation is also extended for geometrically nonlinear analysis of plates [36]. Then, the laminated plates with complicated cutouts were investigated for buckling and free vibration analysis by the combination of the new isogeometric formulation and level-set method [37]. These literatures showed the superior of the NURBS on geometric modeling on the conventional basis functions. Meanwhile, the simple first order shear deformation theory were also integrated with the meshfree moving Kriging method to analyze vibration and deflection of plates with fewer unknown variables [38]. Phung-Van et al. [39] proposed a NURBS formulation to investigate static and dynamic performances of multilayered graphene reinforced plates based on the four-variable refined plate theory. Moreover, IGA was also extended to combine with the Kirchhoff-Love thin-shell theory for analyzing large deformation considering multiple-patch coupling [40] and the inverse analysis of thin shell structures [41]. Based on isogeometric analysis, the level-set topology optimization technique was presented for improving the electromechanical coupling effects in piezoelectric/flexoelectric materials, which contribute towards the design and optimization of micro and nano-scale flexoelectric devices [42–44]. Overall, more and more IGA formulations and methods have been proposed for the analysis, design and optimization of smart materials and structures. In this work, for exploring and analyzing the performances of piezoelectric thin-walled nanocomposite plates, the reduced plate theory and IGA are here combined to develop a semi-analytical approach solving wave characteristics, by integrating the advantages of analytical and numerical methods.

In the present paper, a semi-analytical approach combining the Reissner-Mindlin plate theory and IGA is developed to investigate dispersion behaviors of functionally graded graphene reinforced piezoelectric plates. The volume fraction of GPLs follows various layer-wise distributions through the thickness direction. The effective material properties are estimated by the Halpin-Tsai parallel model and the rule of mixture. Based on Hamilton's principle, governing equation of the piezoelectric composite plates considering the transverse shear deformation is derived and parameterized with the NURBS basis functions. A second-order polynomial eigenvalue problem is obtained to solve wave propagation characteristics. Compared with the results in the literature, the present method is validated for the feasibility and accuracy. Besides, a parametric study is carried out to systematically analyze the effects of distribution pattern, volume fraction, piezoelectricity, size variation of GPLs as well as geometric parameters of the plate on dispersion curves.

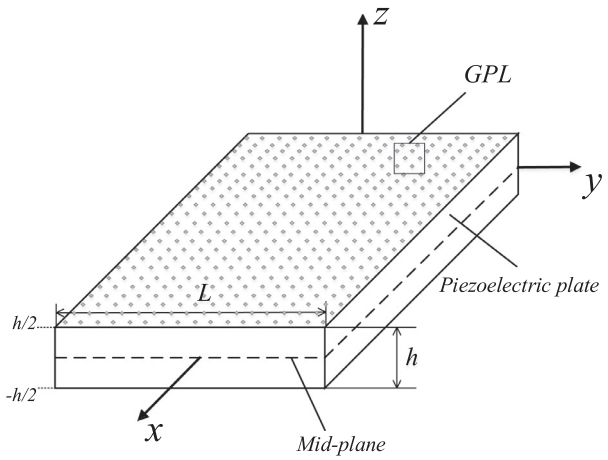

Fig. 1. Schematic configuration of a GPL reinforced composite piezoelectric plate.

2. Basic formulations

In this paper, the piezoelectric composite plate with the reinforcement GPLs and the matrix (polyvinylidene fluoride, PVDF) is considered. The Reissner-Mindlin plate theory with shear deformation and isogeometric analysis with the NURBS basis functions are integrated to develop a semi-analytical approach for wave analysis. The geometry and kinematics of the piezoelectric composite plate are described here. It is assumed that the reference or mid-surface of the plate is continuous, smooth and differentiable. The material property and geometric feature of the plate are invariant along the wave propagation direction. Wave motion of a generic material particle follows the harmonic time-dependent form $\exp(-i\omega t)$, where ω, t and $i=\sqrt{-1}$ denote the angular frequency, time and the imaginary unit, respectively. The related fundamental equations of motion for the piezoelectric composite plate are also represented in this section.

2.1. The Reissner-Mindlin plate theory and kinetic relations

The piezoelectric composite plate is modeled in the Cartesian coordinate system with width L and thickness h, composed of a certain number of layers N. The top and bottom surfaces follow the traction-free and open-circuit boundary conditions. The schematic configuration is shown in Fig. 1. The GPLs disperse through the thickness. Coordinate x represents the propagation direction along the plate. The reference plane or mid-plane is equidistant from both surfaces of the composite plate parallel to the $x-y$ plane. The volume and mid-surface of the plate are represented as V and ∂V.

Considering the first order shear deformation, a generic point in V at a distance z to the mid-plane can be described via the translational displacements $u_0(x, y, z)$, $v_0(x, y, z)$, $w_0(x, y, z)$ and rotations $\alpha_x(x, y, z)$, $\alpha_y(x, y, z)$, based on the Reissner-Mindlin plate theory. The displacement kinematics along three directions are given by

$$\begin{aligned} u(x,y,t) &= u_0(x,y,t) + z\alpha_x(x,y,t) \\ v(x,y,t) &= v_0(x,y,t) + z\alpha_y(x,y,t) \\ w(x,y,t) &= w_0(x,y,t) \end{aligned} \tag{1}$$

where u_0, v_0, and w_0 are the displacements of the reference plane in x, y and z directions, respectively. The rotations α_x and α_y of the cross-section normal to x-axis and y-axis of the plate are independent of coordinate z and their related derivatives equal to zero. Thus, the strain fields are obtained as follows,

$$\begin{aligned} &\varepsilon_{xx} = \varepsilon_{xx}^0 + z\kappa_x,\ \varepsilon_{yy} = \varepsilon_{yy}^0 + z\kappa_y,\ \varepsilon_{zz} = 0 \\ &\varepsilon_{xy} = \varepsilon_{xy}^0 + z\kappa_{xy},\ \varepsilon_{yz} = \frac{\partial w_0}{\partial y} + \alpha_y,\ \varepsilon_{xz} = \frac{\partial w_0}{\partial x} + \alpha_x \end{aligned} \tag{2}$$

where ε_{xx}^0, ε_{yy}^0 and ε_{xy}^0 denote the mid-plane membrane strain components, and the in-plane curvatures components resulted from the transverse shear deformation

$$\kappa_x = \frac{\partial \alpha_x}{\partial x},\quad \kappa_y = \frac{\partial \alpha_y}{\partial y},\quad \kappa_{xy} = \frac{\partial \alpha_x}{\partial y} + \frac{\partial \alpha_y}{\partial x}$$

According to the membrane, bending and shear effects, these strain components are rewritten as the membrane strains in plane

$$\boldsymbol{\varepsilon} = \begin{bmatrix} \frac{\partial u_0}{\partial x} \\ \frac{\partial v_0}{\partial y} \\ \frac{\partial v_0}{\partial x} + \frac{\partial u_0}{\partial y} \end{bmatrix} = \begin{bmatrix} \frac{\partial}{\partial x} & 0 & 0 & 0 & 0 \\ 0 & \frac{\partial}{\partial y} & 0 & 0 & 0 \\ \frac{\partial}{\partial y} & \frac{\partial}{\partial x} & 0 & 0 & 0 \end{bmatrix} \begin{Bmatrix} u_0 \\ v_0 \\ w_0 \\ \alpha_x \\ \alpha_y \end{Bmatrix} \tag{3}$$

the flexural curvatures in plane

$$\boldsymbol{\kappa} = \begin{bmatrix} \frac{\partial \alpha_x}{\partial x} \\ \frac{\partial \alpha_y}{\partial y} \\ \frac{\partial \alpha_y}{\partial x} + \frac{\partial \alpha_x}{\partial y} \end{bmatrix} = \begin{bmatrix} 0 & 0 & 0 & \frac{\partial}{\partial x} & 0 \\ 0 & 0 & 0 & 0 & \frac{\partial}{\partial y} \\ 0 & 0 & 0 & \frac{\partial}{\partial y} & \frac{\partial}{\partial x} \end{bmatrix} \begin{Bmatrix} u_0 \\ v_0 \\ w_0 \\ \alpha_x \\ \alpha_y \end{Bmatrix} \tag{4}$$

and the shear deformations out of plane

$$\boldsymbol{\gamma} = \begin{bmatrix} \frac{\partial w_0}{\partial y} + \alpha_y \\ \frac{\partial w_0}{\partial x} + \alpha_x \end{bmatrix} = \begin{bmatrix} 0 & 0 & \frac{\partial}{\partial y} & 0 & 1 \\ 0 & 0 & \frac{\partial}{\partial x} & 1 & 0 \end{bmatrix} \begin{Bmatrix} u_0 \\ v_0 \\ w_0 \\ \alpha_x \\ \alpha_y \end{Bmatrix} \tag{5}$$

2.2. The generalized constitutive equation for the piezoelectric composite plate

For the piezoelectric composite plate, it is assumed that material property of each layer is homogeneous and it possesses a plane parallel to the mid-plane. The poling direction is along the z-axis direction. The constitutive relations for a piezoelectric layer are expressed as

$$\begin{aligned} \boldsymbol{\sigma} &= \mathbf{Q}\boldsymbol{\epsilon} - \mathbf{e}^T\mathbf{E} \\ \mathbf{D} &= \mathbf{e}\boldsymbol{\epsilon} + \boldsymbol{\mu}\mathbf{E} \end{aligned} \tag{6}$$

where $\boldsymbol{\sigma}$, $\boldsymbol{\epsilon}$ and $\mathbf{D}$ are the stress, strain and the electric displacement vectors, respectively. The elastic tensor $\mathbf{C}$ in three-dimensional form is written as

$$\mathbf{Q} = \begin{bmatrix} Q_{11} & Q_{12} & Q_{13} & 0 & 0 & 0 \\ Q_{21} & Q_{22} & Q_{23} & 0 & 0 & 0 \\ Q_{31} & Q_{32} & Q_{33} & 0 & 0 & 0 \\ 0 & 0 & 0 & Q_{44} & 0 & 0 \\ 0 & 0 & 0 & 0 & Q_{55} & 0 \\ 0 & 0 & 0 & 0 & 0 & Q_{66} \end{bmatrix} \tag{7}$$

The third-order piezoelectric tensor $\mathbf{e}$ representing the mechanical-electric coupling effect and the second-order electric permittivity tensor μ in three-dimensional form is expressed as

$$\mathbf{e} = \begin{bmatrix} 0 & 0 & 0 & 0 & e_{15} & 0 \\ 0 & 0 & 0 & e_{24} & 0 & 0 \\ e_{31} & e_{32} & e_{33} & 0 & 0 & 0 \end{bmatrix}, \quad \boldsymbol{\mu} = \begin{bmatrix} \mu_{11} & 0 & 0 \\ 0 & \mu_{22} & 0 \\ 0 & 0 & \mu_{33} \end{bmatrix} \tag{8}$$

and the electric field intensity $\mathbf{E}$ follows

$$\mathbf{E} = \begin{Bmatrix} E_x \\ E_y \\ E_z \end{Bmatrix} = \begin{Bmatrix} -\frac{\partial}{\partial x} \\ -\frac{\partial}{\partial y} \\ -\frac{\partial}{\partial z} \end{Bmatrix} \varphi \tag{9}$$

in which Q_{ij}, e_{ij} and μ_{ij} $(i, j = 1, 2, ..., 6)$ are denoted with the elastic constants, piezoelectric constants and dielectric constants, respectively, E_i $(i = z, y, z)$ represent the electric intensity along three directions, which are determined by the electric potential φ. The electric potential is independent of coordinate z for the piezoelectric layer, so, the derivative with respect to z is zero.

Furthermore, according to the Reissner-Mindlin plate theory, the normal stress in the thickness direction of plate is negligible while the transverse shear stresses τ_{xz} and τ_{yz} related to coordinate z are not zero. Hence, by combining Eq. (6) and $\sigma_{zz} = 0$, the normal strain ε_{zz} is obtained as

$$\varepsilon_{zz} = \frac{e_{33}E_z - Q_{31}\varepsilon_{xx} - Q_{32}\varepsilon_{yy}}{Q_{33}} \tag{10}$$

Substituting Eq. (10) into Eq. (6) makes the generalized constitutive equations for a piezoelectric layer, as follows

$$\begin{Bmatrix}\sigma_{xx}\\ \sigma_{yy}\\ \tau_{xy}\\ \tau_{yz}\\ \tau_{xz}\end{Bmatrix}=\begin{bmatrix}\bar{Q}_{11} & \bar{Q}_{12} & 0 & 0 & 0\\ \bar{Q}_{21} & \bar{Q}_{22} & 0 & 0 & 0\\ 0 & 0 & \bar{Q}_{66} & 0 & 0\\ 0 & 0 & 0 & \bar{Q}_{44} & 0\\ 0 & 0 & 0 & 0 & \bar{Q}_{55}\end{bmatrix}\begin{Bmatrix}\varepsilon_{xx}\\ \varepsilon_{yy}\\ \gamma_{xy}\\ \gamma_{yz}\\ \gamma_{xz}\end{Bmatrix}-\begin{bmatrix}0 & 0 & \bar{e}_{31}\\ 0 & 0 & \bar{e}_{32}\\ 0 & 0 & 0\\ 0 & \bar{e}_{24} & 0\\ \bar{e}_{15} & 0 & 0\end{bmatrix}\begin{Bmatrix}E_x\\ E_y\\ E_z\end{Bmatrix} \tag{11}$$

$$\begin{Bmatrix}D_x\\ D_y\\ D_z\end{Bmatrix}=\begin{bmatrix}0 & 0 & 0 & 0 & \bar{e}_{15}\\ 0 & 0 & 0 & \bar{e}_{24} & 0\\ \bar{e}_{31} & \bar{e}_{32} & 0 & 0 & 0\end{bmatrix}\begin{Bmatrix}\varepsilon_{xx}\\ \varepsilon_{yy}\\ \gamma_{xy}\\ \gamma_{yz}\\ \gamma_{xz}\end{Bmatrix}+\begin{bmatrix}\bar{\mu}_{11} & 0 & 0\\ 0 & \bar{\mu}_{22} & 0\\ 0 & 0 & \bar{\mu}_{33}\end{bmatrix}\begin{Bmatrix}E_x\\ E_y\\ E_z\end{Bmatrix} \tag{12}$$

where the reduced elastic and piezoelectric coupling constants

$$\begin{aligned}&\bar{Q}_{11}=Q_{11}-\frac{Q_{13}Q_{31}}{Q_{33}},\ \bar{Q}_{12}=Q_{12}-\frac{Q_{13}Q_{32}}{Q_{33}},\ \bar{e}_{31}=e_{31}-\frac{Q_{13}e_{33}}{Q_{33}}\\ &\bar{Q}_{21}=Q_{21}-\frac{Q_{23}Q_{31}}{Q_{33}},\ \bar{Q}_{22}=Q_{22}-\frac{Q_{23}Q_{32}}{Q_{33}},\ \bar{e}_{32}=e_{32}-\frac{Q_{23}e_{33}}{Q_{33}}\\ &\bar{Q}_{66}=Q_{66},\ \bar{Q}_{44}=Q_{44},\ \bar{Q}_{55}=Q_{55},\ \bar{e}_{15}=e_{15},\ \bar{e}_{24}=e_{24}\end{aligned} \tag{13}$$

and the dielectric constants

$$\bar{\mu}_{11}=\mu_{11},\ \bar{\mu}_{22}=\mu_{22},\ \bar{\mu}_{33}=\mu_{33}+\frac{e_{33}e_{33}}{Q_{33}} \tag{14}$$

It is noted that the above formulations are for a piezoelectric layer. For the functionally graded graphene reinforced piezoelectric composite plate, the in-plane force, moment and transverse shear force resultants can be integrated along the plate thickness direction, that is these resultants are sum of the corresponding resultants of each layer. They are obtained as

$$\mathbf{N}_m=\int_{-h/2}^{h/2}\begin{Bmatrix}\sigma_{xx}\\ \sigma_{yy}\\ \sigma_{xy}\end{Bmatrix}dz=\mathbf{A}\boldsymbol{\varepsilon}+\mathbf{B}\boldsymbol{\kappa}-\mathbf{C}\mathbf{E} \tag{15}$$

$$\mathbf{M}_b=\int_{-h/2}^{h/2}\begin{Bmatrix}\sigma_{xx}\\ \sigma_{yy}\\ \sigma_{xy}\end{Bmatrix}zdz=\mathbf{B}\boldsymbol{\varepsilon}+\mathbf{D}\boldsymbol{\kappa}-\mathbf{G}^{\mathbf{T}}\mathbf{E} \tag{16}$$

$$\mathbf{T}_s=K_s\int_{-h/2}^{h/2}\begin{Bmatrix}\tau_{yz}\\ \tau_{xz}\end{Bmatrix}dz=\mathbf{F}\boldsymbol{\gamma}-\mathbf{H}^{\mathbf{T}}\mathbf{E} \tag{17}$$

$$\mathbf{q}_e=\int_{-h/2}^{h/2}\begin{Bmatrix}D_x\\ D_y\\ D_z\end{Bmatrix}dz=\mathbf{C}\boldsymbol{\varepsilon}+\mathbf{H}\boldsymbol{\gamma}+\mathbf{Z}\mathbf{E} \tag{18}$$

where $\mathbf{N}_m=\{N_x,N_y,N_{xy}\}^T$ represents the in-plane force resultant, $\mathbf{M}_b=\{M_x,M_y,M_{xy}\}^T$ is the bending and twisting moment resultant, $\mathbf{T}_s=\{T_{yz},T_{xz}\}^T$ denotes the shear force resultant and $\mathbf{q}_e=\{q_x,q_y,q_z\}^T$ is the electric displacement, K_s is the shear correction factor accounting for the uniform distribution of transverse shear stress in the thickness direction for each layer, which is set as 5/6. The related coefficient matrices are expressed as

$$(\mathbf{A},\mathbf{B},\mathbf{D},\mathbf{F})=\int_{-h/2}^{h/2}(\mathbf{Q}_1,z\mathbf{Q}_1,z^2\mathbf{Q}_1,K_s\mathbf{Q}_2)dz \tag{19}$$

$$(\mathbf{C},\mathbf{G},\mathbf{H},\mathbf{Z})=\int_{-h/2}^{h/2}(\mathbf{e}_1,z\mathbf{e}_1,\mathbf{e}_2,\boldsymbol{\mu}_1)dz \tag{20}$$

with the subblock matrices of the elastic matrix, piezoelectric coupling matrix and dielectric matrix, as follows

$$\mathbf{Q}_1=\begin{bmatrix}\bar{Q}_{11} & \bar{Q}_{12} & 0\\ \bar{Q}_{21} & \bar{Q}_{22} & 0\\ 0 & 0 & \bar{Q}_{66}\end{bmatrix},\ \mathbf{Q}_2=\begin{bmatrix}\bar{Q}_{44} & 0\\ 0 & \bar{Q}_{55}\end{bmatrix} \tag{21}$$

and

$$\mathbf{e}_1=\begin{bmatrix}0 & 0 & 0\\ 0 & 0 & 0\\ \bar{e}_{31} & \bar{e}_{32} & 0\end{bmatrix},\ \mathbf{e}_2=\begin{bmatrix}0 & \bar{e}_{15}\\ \bar{e}_{24} & 0\\ 0 & 0\end{bmatrix},\ \boldsymbol{\mu}_1=\begin{bmatrix}\bar{\mu}_{11} & 0 & 0\\ 0 & \bar{\mu}_{22} & 0\\ 0 & 0 & \bar{\mu}_{33}\end{bmatrix} \tag{22}$$

Table 1
Mechanical properties of GPL and PVDF.

GPL	$E_G = 1.01$ TPa	$\nu_G = 0.186$	$\rho_G = 1920$ kg/m^3
PVDF	$E_M = 1.44$ GPa	$\nu_M = 0.29$	$\rho_M = 800$ kg/m^3

Table 2
Piezoelectric and dielectric constants of PVDF.

$e_{31,M}$	$e_{32,M}$	$e_{33,M}$	$e_{24,M}$	$e_{15,M}$
32.075×10^{-3}	-4.07×10^{-3}	-21.19×10^{-3}	-12.65×10^{-3}	-15.93×10^{-3}
$\mu_{11,M}$	$\mu_{22,M}$	$\mu_{33,M}$		
53.985×10^{-12}	66.375×10^{-12}	59.295×10^{-12}		

* Units: $e_{ij,M}(C/m^2)$, $\mu_{ij,M}(F/m)$.

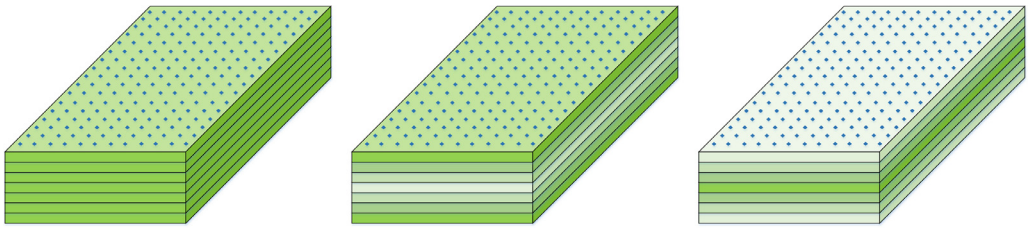

Fig. 2. The distribution patterns of GPL/PVDF in the nanocomposite plate.

From Eqs. (15)–(18) the generalized resultants are expressed in the matrix form as

$$\mathbf{P} = \boldsymbol{\Theta}\boldsymbol{\Sigma} \tag{23}$$

with

$$\mathbf{P} = \{\mathbf{N_m} \quad \mathbf{M_b} \quad \mathbf{T_s} \quad \mathbf{q_e}\}^T, \quad \boldsymbol{\Sigma} = \{\boldsymbol{\varepsilon} \quad \boldsymbol{\kappa} \quad \boldsymbol{\gamma} \quad \mathrm{E}\}^T$$

$$\boldsymbol{\Theta} = \begin{bmatrix} A & B & 0 & -C^T \\ B & D & 0 & -G^T \\ 0 & 0 & F & -H^T \\ C & G & H & Z \end{bmatrix}, \quad \bar{\boldsymbol{\Theta}} = \begin{bmatrix} A & B & 0 & -C^T \\ B & D & 0 & -G^T \\ 0 & 0 & F & -H^T \\ -C & -G & -H & -Z \end{bmatrix}$$

in which, $\mathbf{P}$ is the resultant vector and Σ is the generalized strain vector, Θ and $\bar{\Theta}$ denote the coefficient matrices.

2.3. Effective material properties

In this work, the functionally graded composite plate consist of N_L layer of graphene reinforced piezoelectric homogeneous plate with the PVDF matix, which is assumed to be uniformly dispersed by the GPLs. The mechanical properties of GPL and PVDF [11,16] are listed in Table 1 and the piezoelectric and dielectric constants of PVDF [45] are shown in Table 2. Fig. 2 shows three types of distribution patterns U, X, O of GPL/PVDF following a layer-wise variation across the thickness of the nanocomposite plate. Pattern U represents the uniformly distribution of GPLs in the isotropic homogeneous piezoelectric composite plate, Pattern X and O demonstrate the symmetric distributions of the GPLs as the volume fraction increases and decreases layer by layer from the middle to the surface.

According to reference [24], the variations of the GPL volume fraction for three types of patterns are described by

Pattern U:

$$f_i = f_{GPL} \tag{24}$$

Pattern X:

$$\begin{aligned} f_i &= \left(\frac{N}{2} + 1 - i\right) f^* \qquad \text{if} \quad i \le \frac{N}{2} \\ f_i &= \left(i - \frac{N}{2}\right) f^* \qquad \text{if} \quad i > \frac{N}{2} \end{aligned} \tag{25}$$

Pattern O:

$$f_i = if^* \qquad \text{if} \quad i \le \frac{N}{2}$$
$$f_i = (N+1-i)f^* \qquad \text{if} \quad i > \frac{N}{2} \tag{26}$$

with

$$f^* = \frac{2}{1+\frac{N}{2}} f_{GPL}$$

where f_i $(i = 1, 2, ..., N_L)$, f^* and f_{GPL} are the volume fraction of GPLs for the ith layer, the average volume fraction of GPLs and the total volume fraction in composite plate.

Besides, it is assumed that the GPL nanofillers are perfectly bonded with the matrix PVDF. The existing study [46] indicates that the Halpin-Tsai model is more accurate to predict the tensile modulus of the composites with the GPL nanofillers and polymer matrix, compared with the Mori-Tanaka model. Nandi et al. [47] pointed out that the Young's modulus of the graphene reinforced PVDF composites can be calculated by the Halpin-Tsai parallel model when the GPL volume fraction is below 1%. Meanwhile, the experimental results [48] reported that the piezoconductive effect of the graphenes, which highly depends on the layer number of the graphenes. The piezoelectric and dielectric properties of the graphene nanofillers can be supposed as β times larger than that of the PVDF [24], and β is called the piezoelectric multiple. Therefore, the layer-dependent material modulus of the piezoelectric composite plate are determined by

$$E_{Ci} = \frac{1+\frac{2l_{GPL}}{3t_{GPL}}\eta_L f_i}{1-\eta_L f_i} E_M \tag{27}$$

with

$$\eta_L = \frac{\frac{E_G}{E_M}-1}{\frac{E_G}{E_M}+\frac{2l_{GPL}}{3t_{GPL}}}$$

and the effective material properties by the rule of mixtures are expressed as follows

$$\begin{aligned} \rho_i &= \rho_G f_i + \rho_M(1-f_i) \\ \nu_i &= \nu_G f_i + \nu_M(1-f_i) \\ e_i &= e_G f_i + e_M(1-f_i) \\ \mu_i &= \mu_G f_i + \mu_M(1-f_i) \end{aligned} \tag{28}$$

where E_{Ci}, E_G and E_M are Young's moduli of the composite, graphene and polymer matrix, respectively, l_{GPL} and t_{GPL} represent the average length, thickness of GPL, ρ_i, ν_i, e_i and μ_i denote the effective mass density, Poisson's ratio, piezoelectric constant and dielectric constant of the ith layer for the nanocomposite, ρ_G (ρ_M), ν_G (ν_M), e_G (e_M) and μ_G (μ_M) are the effective mass density, Poisson's ratio, piezoelectric constant and dielectric constant of the GPL (polymer matrix), respectively.

3. Wave equations for graphene-reinforced piezoelectric composite plates

In this section the NURBS basis function is briefly reviewed on its construction and description of solution fields in isogeometric analysis. Later on, elastic wave equation for the piezoelectric nanocomposite plate is derived and parameterized by the basis functions.

3.1. NURBs basis function

The NURBS basis functions are linearly combined by piecewise polynomial B-spline basis functions and control points which can be visualized in coordinate space, which have been the most prevalent geometric representation. Compared with the Lagrangian polynomials, the NURBS basis functions can exactly describe the geometry and physical fields so that the discretization error and computational cost can be efficiently voided and improved in virtue of the high smoothness and continuity [32]. This section represents the basic concepts of the NURBS basis functions and the works [31] can be referred to for more details about isogeometric analysis.

In the parameter space in $0 \le \xi \le 1$, a non-decreasing knot vector is utilized to construct a B-spline and the vector is defined by a real sequence $\Xi = [\xi_1, \xi_2, \cdots, \xi_{n+p+1}]$, where n and p are the number of basis functions and the order. In order to satisfy the interpolating characteristics at boundaries, the first and last knots of knot vector repeat $(p+1)$ times, respectively. The parameter space is partitioned by the knots with elements. With a knot vector, the B-spline basis functions are expressed by the CoxCDe Boor recursive formula [49]

$$N_{i,0}(\xi) = \begin{cases} 1, & if \quad \xi_i \leqslant \xi < \xi_{i=1} \\ 0, & otherwise \end{cases}$$
$$N_{i,p}(\xi) = \frac{\xi-\xi_i}{\xi_{i+p}-\xi_i} N_{i,p-1}(\xi) + \frac{\xi_{i+p+1}-\xi}{\xi_{i+p+1}-\xi_{i+1}} N_{i+1,p-1}(\xi) \qquad for \quad p \geqslant 1 \tag{29}$$

Given n basis functions and control points $\boldsymbol{a}_i$ $(i = 1, 2, ..., n)$, the physical field are described by

$$\boldsymbol{a} = \sum_{i=1}^{Cpts} \mathbf{R}_i^p(\mathbf{r}(\boldsymbol{\xi}))\boldsymbol{a}_i \tag{30}$$

with the basis function for one-dimensional problem

$$\mathbf{R}_i^p(\xi) = \frac{N_i^p(\xi)\omega_i}{\sum_{j=1}^{n} N_j^p(\xi)\omega_j}$$

where *Cpts* denotes the number of control points in isogeometric parametric mesh and ω_i is the weight value for the ith basis function, ξ represents the knot, i.e. the parametric coordinate in the parametric space and $\mathbf{r}$ represents the physical cartesian coordinate, $\mathbf{a}$ and $\mathbf{a}_i$ are the interpolated physical vector and the physical vector of the ith control point.

3.2. Parameterized equation for dispersion characteristics using a semi-analytical approach

As we know, the mechanical and electric response are coupled in the linear piezoelectric problem. When elastic wave propagates in a piezoelectric composite plate, it is assumed that the generalized displacements depend on $e^{-\mathcal{I}(\omega t - kx)}$, where t, ω, k and $\mathcal{I}$ denote the time, angular frequency, wavenumber and the imaginary unit. The generalized displacement vector is expressed as a Fourier series, that is

$$\mathbf{u}(y, t) = \mathbf{U}(y, t)e^{-\mathcal{I}(\omega t - kx)} \tag{31}$$

with

$$\mathbf{u} = [u_0, v_0, w_0, \alpha_x, \alpha_y, \varphi]^T$$

where $\mathbf{U}$ is the amplitude of the generalized displacements, namely physical field including the displacement and the electric potential. The related variational of displacements are expressed as

$$\delta\mathbf{u}(y, t) = \delta\mathbf{U}(y, t)e^{-\mathcal{I}(\omega t - kx)} \tag{32}$$

According to the plate theory, the geometry of the cross section of the plate is described by one-dimensional NURBS basis function. The coordinate of a generic particle is represented by the coordinates of control points and the NURBS basis function, as follows

$$\boldsymbol{y} = \sum_{i=1}^{Cpts} \mathbf{R}_i^p(\boldsymbol{y}(\boldsymbol{\xi}))\boldsymbol{y}_i \tag{33}$$

In the parametric space each element is determined by two adjacent knots, which can be described by the mapping from the parent element to the parametric space to the physical space. J_1 represents the Jacobian determinant for mapping from the parametric space to the physical space and the transformation between two types of coordinates is given by

$$\left[\frac{\partial}{\partial\xi}\right] = J_1\left[\frac{\partial}{\partial\mathbf{y}}\right] \tag{34}$$

with

$$J_1 = \left|\frac{\partial\mathbf{y}}{\partial\xi}\right| = \mid \mathbf{R}_{i,\xi}^p y_i \mid$$

J_2 is the Jacobian determinant for mapping from the parent space $\xi \in [-1, 1]$ to the parametric space and for the ith element, the Jacobian determinant $J_2 = \mid (\xi_{i+1} - \xi_i)/2 \mid$. Therefore, we get the global mapping determinant $J = J_1 * J_2$.

For the piezoelectric composite plate, the total potential energy is obtained by integrating the strain energy density and the electrostatic energy density functions, as follows

$$\begin{aligned}\Pi_{pot} &= \int_\Omega \left(\boldsymbol{\varepsilon}^T\mathbf{N}_m + \boldsymbol{\kappa}^T\mathbf{M}_b + \boldsymbol{\gamma}^T\mathbf{T}_s - \mathbf{E}^T\mathbf{q}_e\right)d\Omega \\ &= \int_\Omega \boldsymbol{\Sigma}^T\bar{\boldsymbol{\Theta}}\boldsymbol{\Sigma}d\Omega\end{aligned} \tag{35}$$

The kinetic energy can be divided in to two parts containing the translational motion and the rotational motion

$$\begin{aligned}\Pi_{kin} &= \frac{1}{2}\int_\Omega \left(\mathbf{I}\dot{\mathbf{u}}^2\right)d\Omega \\ &= \frac{1}{2}\int_\Omega \left(\mathbf{I}_0\dot{\mathbf{u}}^2 + 2\mathbf{I}_1\dot{\mathbf{u}}\dot{\boldsymbol{\alpha}} + \mathbf{I}_2\dot{\boldsymbol{\alpha}}^2\right)d\Omega\end{aligned} \tag{36}$$

where the dot (.) indicates the partial derivative with respect to time t, and the inertia terms are given by

$$\mathbf{I} = \begin{bmatrix} \mathbf{I}_0 & \mathbf{I}_{12} & \mathbf{0} \\ \mathbf{I}_{12}^T & \mathbf{I}_2 & \mathbf{0} \\ \mathbf{0} & \mathbf{0} & \mathbf{0} \end{bmatrix}, \mathbf{I}_{12} = \begin{bmatrix} \mathbf{I_1} & \mathbf{0} \\ \mathbf{0} & \mathbf{I_1} \\ \mathbf{0} & \mathbf{0} \end{bmatrix}$$
$$\mathbf{I_0} = \mathbf{diag}(I_0, I_0, I_0), \mathbf{I_1} = \mathbf{diag}(I_1, I_1), \mathbf{I_2} = \mathbf{diag}(I_2, I_2)$$
$$I_0 = \int_{-h/2}^{h/2} \rho(z)\mathrm{d}z, I_1 = \int_{-h/2}^{h/2} \rho(z)z\mathrm{d}z, I_2 = \int_{-h/2}^{h/2} \rho(z)z^2\mathrm{d}z \tag{37}$$

According to Eq. (31) the strain tensor is expressed as

$$\mathbf{\Sigma} = (\mathbf{L_1} + \mathcal{I}k\mathbf{L_2})\bar{\mathbf{u}} \tag{38}$$

with

$$\mathbf{L}_1 = \begin{bmatrix} \mathbf{L}_\varepsilon^1 & 0 \\ \mathbf{L}_\kappa^1 & 0 \\ \mathbf{L}_\gamma^1 & 0 \\ 0 & \mathbf{L}_E^1 \end{bmatrix}, \quad \mathbf{L}_2 = \begin{bmatrix} \mathbf{L}_\varepsilon^2 & 0 \\ \mathbf{L}_\kappa^2 & 0 \\ \mathbf{L}_\gamma^2 & 0 \\ 0 & \mathbf{L}_E^2 \end{bmatrix}$$

and

$$\mathbf{L}_\varepsilon^1 = \begin{bmatrix} 0 & 0 & 0 & 0 & 0 \\ 0 & \frac{\partial}{\partial y} & 0 & 0 & 0 \\ \frac{\partial}{\partial y} & 0 & 0 & 0 & 0 \end{bmatrix} \mathbf{L}_\kappa^1 = \begin{bmatrix} 0 & 0 & 0 & 0 & 0 \\ 0 & 0 & 0 & 0 & \frac{\partial}{\partial y} \\ 0 & 0 & 0 & \frac{\partial}{\partial y} & 0 \end{bmatrix} \mathbf{L}_\gamma^1 = \begin{bmatrix} 0 & 0 & \frac{\partial}{\partial y} & 0 & 1 \\ 0 & 0 & 0 & 1 & 0 \end{bmatrix} \mathbf{L}_E^1 = \begin{bmatrix} 0 \\ -\frac{\partial}{\partial y} \\ 0 \end{bmatrix}$$

$$\mathbf{L}_\varepsilon^2 = \begin{bmatrix} 1 & 0 & 0 & 0 & 0 \\ 0 & 0 & 0 & 0 & 0 \\ 0 & 1 & 0 & 0 & 0 \end{bmatrix} \mathbf{L}_\kappa^2 = \begin{bmatrix} 0 & 0 & 1 & 0 & 0 \\ 0 & 0 & 0 & 0 & 0 \\ 0 & 0 & 0 & 1 & 0 \end{bmatrix} \mathbf{L}_\gamma^2 = \begin{bmatrix} 0 & 0 & 0 & 0 & 0 \\ 0 & 0 & 1 & 0 & 0 \end{bmatrix} \mathbf{L}_E^2 = \begin{bmatrix} -1 \\ 0 \\ 0 \end{bmatrix}$$

Based on Hamilton's principle, the variation of the energy functional must vanish for all $\bar{\mathbf{u}}$ if the system is in equilibrium, that is

$$\begin{aligned} \delta\Pi &= \delta\Pi_{kin} - \delta\Pi_{pot} \\ &= \omega^2\delta\mathbf{U}^T \int_\Omega \mathbf{R}^T\mathbf{I}^T\mathbf{R}d\Omega\mathbf{U} - \delta\mathbf{U}^T \int_\Omega (\mathbf{B}_1 + \mathcal{I}k\mathbf{B}_2)^T \bar{\Theta}^T (\mathbf{B}_1 + \mathcal{I}k\mathbf{B}_2)d\Omega\mathbf{U} \\ &= \delta\mathbf{U}^T[\mathbf{K}_1 + \mathcal{I}k(\mathbf{K}_2 - \mathbf{K}_2^T) + k^2\mathbf{K}_3 - \omega^2\mathbf{M}]\mathbf{U} = 0 \end{aligned} \tag{39}$$

and

$$\mathbf{K}_1 = \int_{\Omega_e} \mathbf{R}^T\mathbf{L}_1^T\bar{\mathbf{\Theta}}\mathbf{L}_1\mathbf{R}|J_1||J_2|d\xi, \quad \mathbf{K}_2 = \int_{\Omega_e} \mathbf{R}^T\mathbf{L}_1^T\bar{\mathbf{\Theta}}\mathbf{L}_2\mathbf{R}|J_1||J_2|d\xi$$
$$\mathbf{K}_3 = \int_{\Omega_e} \mathbf{R}^T\mathbf{L}_2^T\bar{\mathbf{\Theta}}\mathbf{L}_2\mathbf{R}|J_1||J_2|d\xi, \quad \mathbf{M} = \int_{\Omega_e} \mathbf{R}^T\mathbf{I}\mathbf{R}|J_1||J_2|d\xi$$

Considering the arbitrary variations of $\delta\mathbf{U}^T$, Eq. (39) must be satisfied such that

$$[\mathbf{K}_1 + \mathcal{I}k(\mathbf{K}_2 - \mathbf{K}_2^T) + k^2\mathbf{K}_3 - \omega^2\mathbf{M}]\mathbf{U} = 0 \tag{40}$$

which demonstrates the reduction of geometric dimensionality by taking the Fourier transform from the space domain x into the wavenumber domain k. Here is is an second-order polynomial eigenvalue problem and the solution is obtained by referring to the reference [30]. For any given angular frequency ω, the wavenumbers appear in pairs representing positive- and negative- going waves and the eigenvectors describe the wave shapes. According to the definition of group velocity and the derivative with respect k for Eq. (40), the expression is

$$\mathbf{U}^H\left[\mathcal{I}(\mathbf{K}_2 - \mathbf{K}_2{}^T) + 2k\mathbf{K}_3 - 2\omega\frac{\partial\omega}{\partial k}\mathbf{M}\right]\mathbf{U} = 0 \tag{41}$$

thus, the frequency-dependent group velocity is calculated by

$$c_g = \frac{\mathbf{U}^H(\mathcal{I}(\mathbf{K}_2 - \mathbf{K}_2{}^T) + 2k\mathbf{K}_3)\mathbf{U}}{2\omega\mathbf{U}^H\mathbf{M}\mathbf{U}} \tag{42}$$

where $\mathbf{U}$ is the eigenvector and the superscript H denotes the complex conjugate transpose.

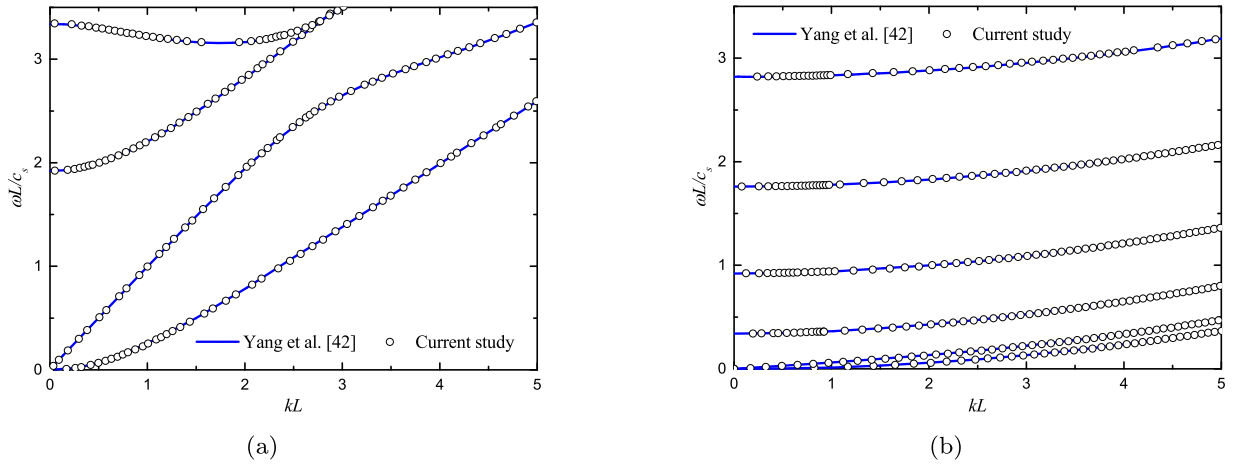

Fig. 3. Frequency spectra based on the Reissner-Mindlin plate theory. (a) In-plane modes; (b) Flexural modes.

Table 3
Convergence analysis of p- and h-refinements on calculation of dispersive properties.

Order elevation	Knot insertion	1	2	3	4	5
p=2	5	0.5004	1.4983	2.5778	5.1357	5.8377
	10	0.5005	1.4984	2.7628	5.1566	5.8432
	20	0.5005	1.4984	2.7817	5.1636	5.8447
	30	0.5005	1.4984	2.7843	5.1648	5.8450
	50	0.5005	1.4984	2.7850	5.1651	5.8451
	100	0.5005	1.4984	2.7851	5.1652	5.8451
p=4	5	0.5005	1.4984	2.7671	5.1582	5.8434
	10	0.5005	1.4984	2.7831	5.1642	5.8449
	20	0.5005	1.4984	2.7851	5.1652	5.8451
	30	0.5005	1.4984	2.7852	5.1652	5.8451
	50	0.5005	1.4984	2.7852	5.1652	5.8451
	100	0.5005	1.4984	2.7852	5.1652	5.8451
p=6	5	0.5005	1.4984	2.7797	5.1651	5.8445
	10	0.5005	1.4984	2.7850	5.1647	5.8451
	20	0.5005	1.4984	2.7852	5.1652	5.8451
	30	0.5005	1.4984	2.7852	5.1652	5.8451
	50	0.5005	1.4984	2.7852	5.1652	5.8451
	100	0.5005	1.4984	2.7852	5.1652	5.8451

4. Numerical results and discussion

4.1. Validation and convergence analysis

In order to confirm the reliability, firstly, it is necessary to validate the proposed semi-analytical approach. An isotropic homogeneous plate is analyzed for wave characteristics considering the first order shear deformation. The plate is made from polymethyl methacrylate (PMMA) with Young's modulus $E_p = 2.5$GPa, Poisson's ratio $\nu_p = 0.34$ and mass density $\rho_p = 1190\text{kg/m}^3$ [50]. Without loss of generality, the frequency and wavenumber are nondimensionalized as $\omega L/\sqrt{E_p/\rho_p}$ and kL. The width L and height h of the plate are set 0.1 and 0.005 (the height to width ratio $s = 20$). By using the present method, the frequency spectra of in-plane and flexural wave modes are shown respectively in Fig. 3(a) and (b) and the results are compared to that by Yang et al. [51], which combined the state space formulation and the method of reverberation-ray matrix (MRRM) offering unconditional numerical stability. It is clearly noted that the results of both are identical, which gives confidence that the semi-analytical approach, based on the Reissner-Mindlin plate theory and isogeometric analysis, is reasonable and accurate for computing wave characteristics.

Besides, a piezoelectric composite plate without GPLs reinforcements is considered for analysing convergence of the present approach. The width to height ratio $s = 20$, the layer number $N_L = 1$ and the material properties of the plate are assumed as that in Tables 1 and 2. Table 3 lists dispersive properties of the first five propagating modes in piezoelectric composite plate at the nondimensional frequency 0.5. It is known that order elevation and knot insertion are two primitive refinements (p and h refinements are similar to that of the classical finite element analysis). The dispersive results for various p-refinement and h-refinement in modeling are compared here. For a certain order, dispersive results increase as

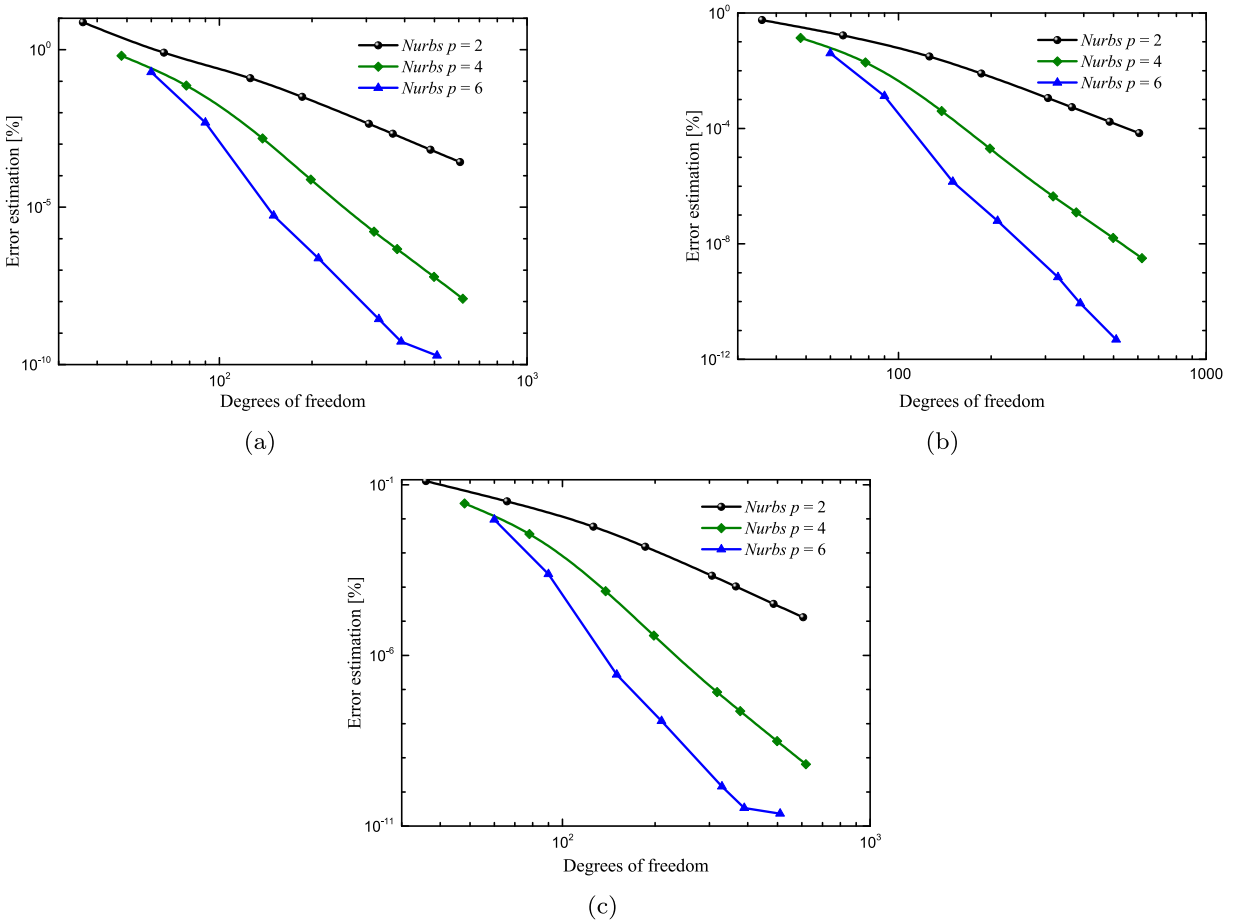

Fig. 4. Error estimation of dispersive results of three modes 3, 4 and 5 the NURBS in IGA and Lagrs in FEA. (a) Mode 3; (b) Mode 4; (c) Mode 5.

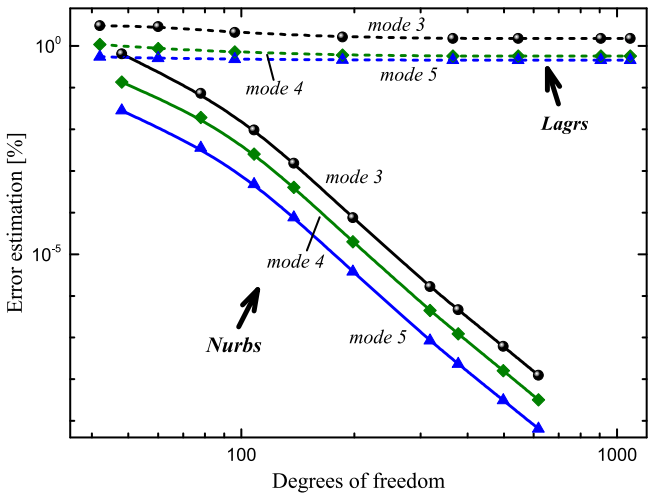

Fig. 5. Comparison of relative errors of both basis functions with order $p = 4$ and various parameters of h-refinement (the dashed and solid lines represent the results of the semi-analytical approaches based on Lagrangian shape functions in FEA and the NURBS in IGA, respectively).

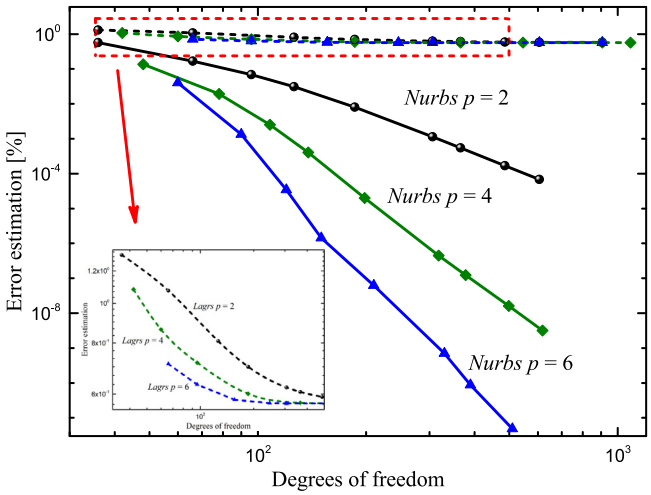

Fig. 6. Comparison of relative errors of both basis functions with different orders and various parameters of *h*-refinement (the dashed and solid lines represent the results of the semi-analytical approaches based on Lagrangian shape functions in FEA and the NURBS in IGA, respectively).

Table 4
Convergence of dimensionless dispersive wavenumbers of different wave modes in functionally graded piezoelectric composite plates reinforced with GPLs at $\Omega = 0.5$.

N_L	Pattern U			Pattern X			Pattern O		
	3	4	5	3	4	5	3	4	5
4	1.9347	4.6234	5.3645	1.7493	4.5185	5.2704	2.1263	4.7384	5.4679
6	1.9347	4.6234	5.3645	1.6884	4.4855	5.2409	2.1922	4.7793	5.5048
8	1.9347	4.6234	5.3645	1.6580	4.4693	5.2264	2.2255	4.8003	5.5237
10	1.9347	4.6234	5.3645	1.6398	4.4597	5.2178	2.2457	4.8131	5.5352
12	1.9347	4.6234	5.3645	1.6277	4.4534	5.2122	2.2592	4.8216	5.5429
20	1.9347	4.6234	5.3645	1.6034	4.4408	5.2009	2.2864	4.8390	5.5585
50	1.9347	4.6234	5.3645	1.5816	4.4296	5.1909	2.3110	4.8548	5.5728
1000	1.9347	4.6234	5.3645	1.5678	4.4225	5.1846	2.3267	4.8649	5.5820

knots insert. With order elevating, all numerical results of five modes based on the semi-analytical approach are converged for insertion of more knots.

For the sake of showing the superiority of the present approach, the NURBS in IGA and Lagrangian shape functions (Lagrs) in finite element analysis (FEA) are used for the convergence analysis. The dispersive results with respect to $p = 6$ and the number of inserted knots 100 are regarded as the reference values for error estimation of computational results. From Table 3, the first two modes are almost invariant with the increase of refinements while the others are very sensitive to order elevation and knot insertion. Mode 3, 4 and 5 are representative to study the convergence and accuracy of the present approach. Firstly, Fig. 4 shows the comparison of error estimations of NURBS with different refinement parameters. From Fig. 4, the convergence can be achieved by regulating *p*-and *h*-refinements, the relative errors decrease monotonously similar to Table 3. It indicates that the dispersive results converge along order elevation and knot insertion. Then, when the order $p = 4$, the error estimation of the NURBS and Lagrangian shape functions are assessed by *h*-refinement in Fig. 5. It is noted that the NURBS lead to lower relative error than the Lagrangian basis functions in FEA, and the convergence rate is rather higher than the latter. Additionally, Fig. 6 represents the comparison of relative errors of both basis functions with different orders and various parameters of *h*-refinement. Changing the orders can improve the convergence of both basis functions, and the NURBS is always superior to the Lagrangian shape functions. As previously mentioned, the calculational precision is enough when the the order $p = 4$ and the number of inserted knots is 30. Therefore, these refinement parameters are also chosen for accurate modeling the functionally graded piezoelectric composite reinforced with GPLs in the following sections.

Table 4 represents dimensionless dispersive wavenumbers of the latter three wave modes in the piezoelectric composite plates at $\Omega = 0.5$. The related parameters of the piezoelectric composite plate are the same as the above except the volume fraction of GPLs $f_{GPL} = 0.1\%$. When layer number $N_L = 1000$, the numerical results can be regarded as the reference. Numerical results of dispersive characteristics for various layer number and three types of distribution patterns are given in Table 4 and the relative errors of dispersive properties are clearly depicted in Fig. 7. For Patter U, the results are not affected by the variation of layer number. For Pattern X or O, the inhomogeneous material distribution has significant influence on propagation characteristics of the flexural wave modes. It is obviously observed that the calculation precision can be

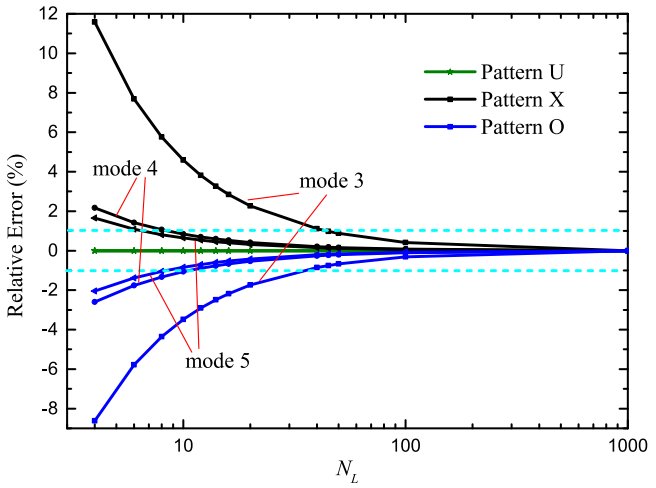

Fig. 7. The effect of layer number N_L on the relative errors of wavenumbers of wave propagating modes for three types of patterns.

efficiently improved as N_L raises and the errors less than or equal to 1% (cyan curve) with respect to the reference results are sufficiently accurate when $N_L \geq 40$.

4.2. Wave dispersion in the functionally graded graphene reinforced piezoelectric composite plate

Wave propagation in the piezoelectric composite plate reinforced with GPLs are presented in terms of several significant parameters. The composite plate is made from polymer matrix PVDF and reinforcement graphene platelets and the corresponding material properties are given in Tables 1 and 2. The length, width and thickness of GPL are measured as $l_{GPL} = 2.5$ μm, $w_{GPL} = 1.5$ μm and $t_{GPL} = 1.5$ nm [21]. Following the discussion in the previous section, the layer number of the composite plate is set as $N_L = 40$.

First of all, dispersive properties of propagating waves in a piezoelectric composite plate with volume fraction $f_{GPL} = 0.1\%$ and the width-to-thickness ratio $L/h = 20$ are displayed in Fig. 5. Graphene platelets are dispersed following Pattern U. Fig. 8(a) exhibits the frequency-spectra curves of the plate, there exist two kinds of wave modes including in-plane modes and flexural modes. Fig. 8(b) and (c) illustrate phase-velocity and group-velocity curves, respectively, which can guide the selection of guided wave modes and excitation frequency of piezoelectric coupling sensors in structural health monitoring. For convenience, the first five flexural wave modes are marked as F_i $(i = 1, 2, ..., 5)$ and the first three in-plane wave modes are signed by P_j $(j = 1, 2, 3)$. In order to demonstrate the effects of some significant parameters, mode P_1, P_2, F_1 and F_3 are employed to represent the propagation characteristics of the in-plane and flexural wave modes.

Fig. 9 displays dispersion behaviors of wave modes in piezoelectric nanocomposite plate and the effects of three types of distribution patterns on wave propagation are shown. It is noted clearly that Pattern X and Pattern O have opposite impacts on frequency spectra and group velocity of the flexural wave modes. The GPLs concentrate on the top and bottom surfaces, which leads to the smaller wavenumbers and higher transmission speed of energy. The influence of graphene concentrated on the middle layer is on the contrary. Besides, the variation of distribution pattern has no influence on wave characteristics of in-plane wave modes.

The effects of volume fraction of GPLs on dispersion curves are depicted in Fig. 10 for the functionally graded graphene reinforced piezoelectric composite plate with Patterns U, X and O, respectively. The variation of volume fraction has great influence on frequency spectra and group velocity of wave modes. Relatively speaking, the flexural dispersion curves are pretty concentrated in the case of Pattern O, which are not sensitive to various volume fraction of GPLs. Fig. 10(a) and (b) illustrate the variation of wave propagation characteristics in the case of Pattern U. It is clearly found that the wavenumbers of in-plane wave modes decrease as the volume fraction of GPLs increases. The energy of wave modes transmits faster and faster. When the volume fraction is below 0.3%, the flexural wave modes also have the similar changes. However, at the high frequencies, the wavenumbers become bigger and the energy transmits slower. Meanwhile, wave characteristics when the graphene distribution follows Patter X and O are shown in Fig. 10(c)–(f) with the same phenomenon. For the purpose of clearly stating the variation of wavenumbers with volume fraction increasing, Fig. 10(g) demonstrates the changing curves of wavenumbers of mode F_1 and F_2 with respect to the volume fraction at the nondimensional frequency $\Omega = 2$. Mode F_1 reduces initially then increases as f_{GPL} raises but Mode F_1 only decreases monotonically.

Fig. 11 shows the influence of the width-to-thickness ratio of the plate (L/h) on dispersion curves of the piezoelectric composite plate. The wave characteristics of flexural wave modes are significantly affected by the ratio. With the increase of the ratio, namely the composite plate becomes wider or thinner, at a certain frequency the wavenumbers get bigger and bigger for the flexural wave modes, and group velocity decreases with the lower speed of transmission of wavepacket and

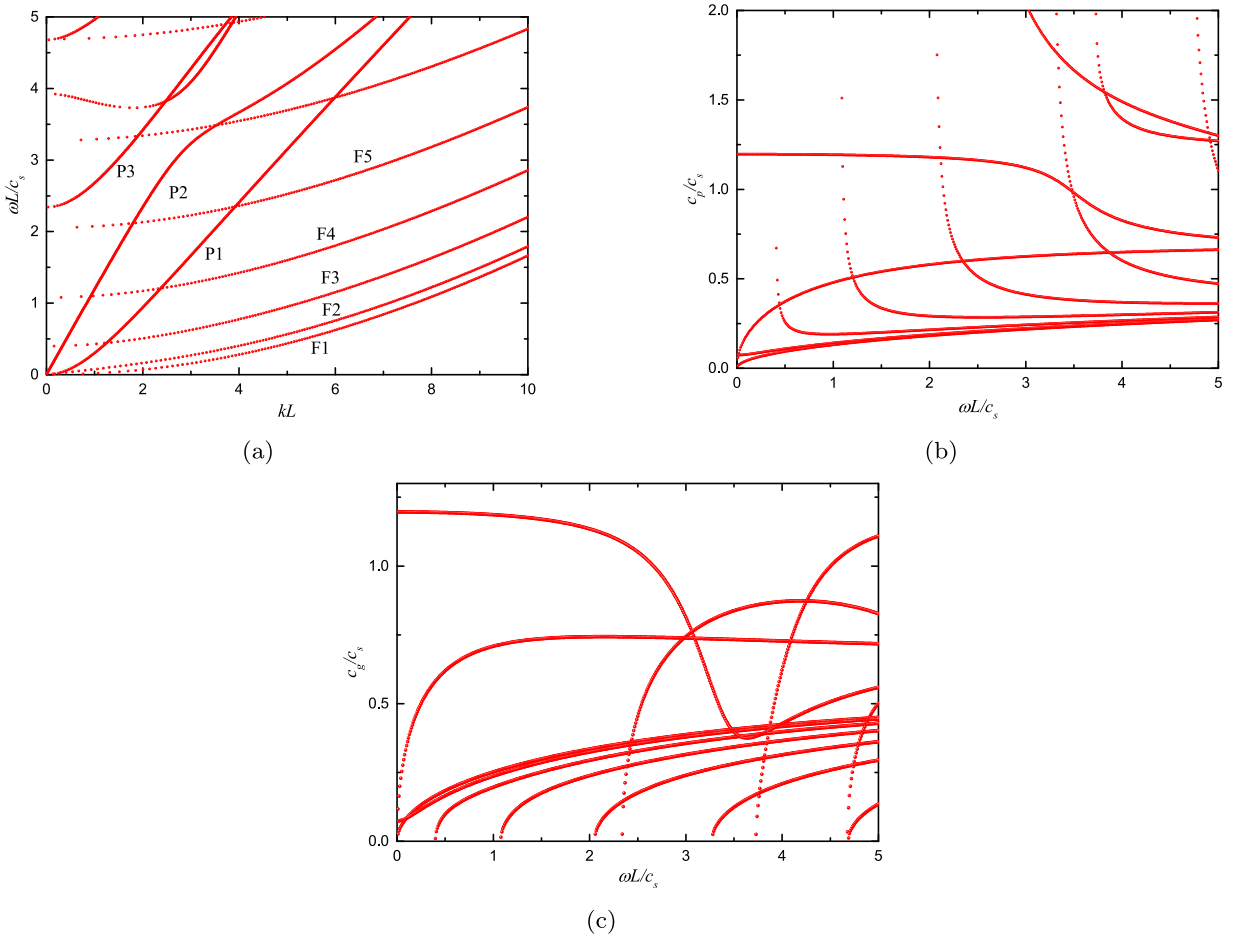

Fig. 8. Dispersion curves of functionally graded piezoelectric composite plates with $f_{GPL} = 0.1\%, L/h = 20, N_L = 40$ and Pattern U. (a) Frequency spectra; (b) Phase velocity; (c) Group velocity.

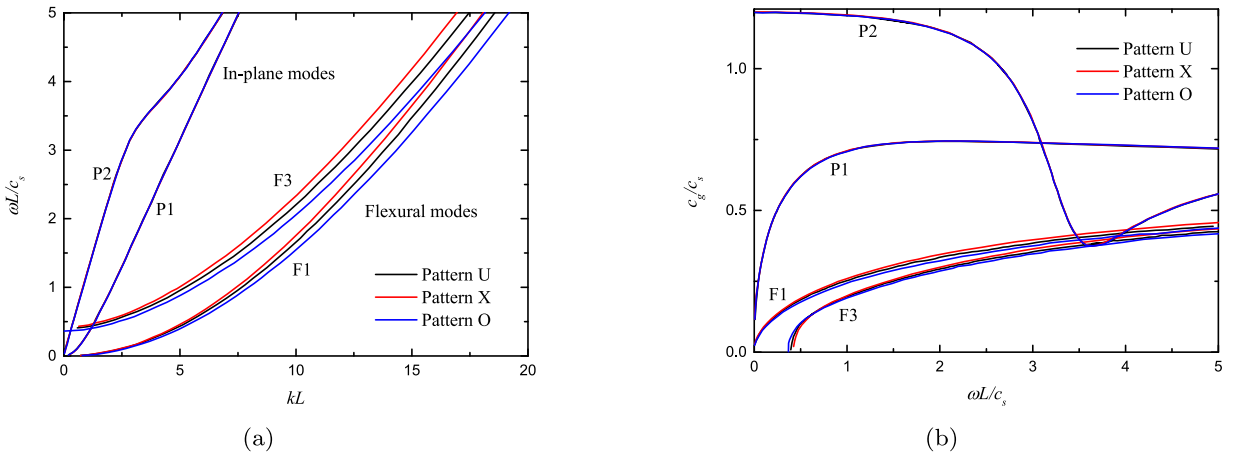

Fig. 9. Variation of dispersion curves of functionally graded piezoelectric composite plates with $f_{GPL} = 0.1\%, L/h = 20, N_L = 40$ for three Patterns. (a) Frequency spectra; (b) Group velocity.

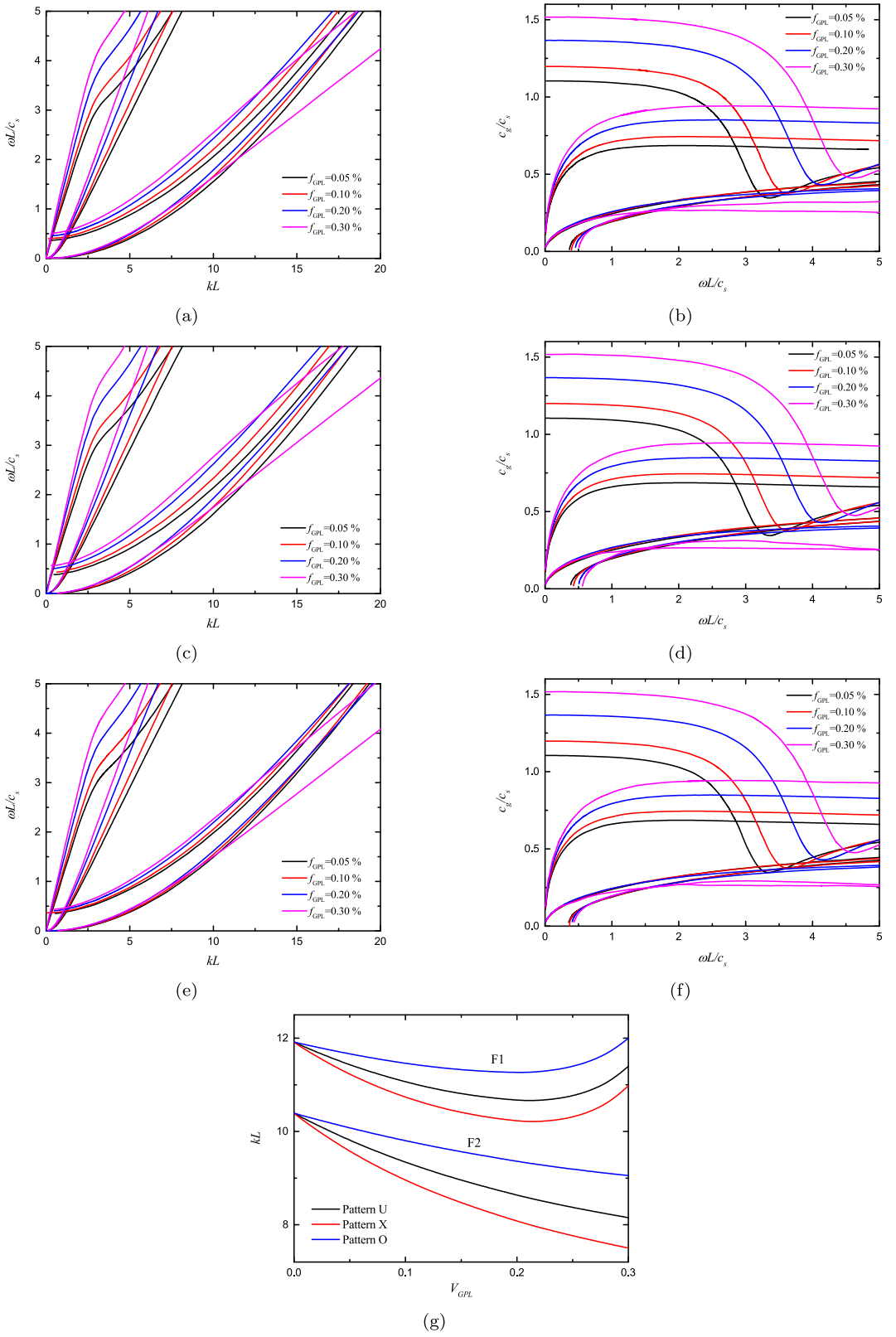

Fig. 10. Influences of volume fraction of the GPLs on dispersive properties in the piezoelectric composite plates with $L/h = 20, N_L = 40$ for Patterns U, X and O. (a) Frequency spectra for Pattern U; (b) Group velocity for Pattern U; (c) Frequency spectra for Pattern X; (d) Group velocity for Pattern X; (e) Frequency spectra for Pattern O; (f) Group velocity for Pattern O; (g) wavenumbers vs volume fraction of the GPL.

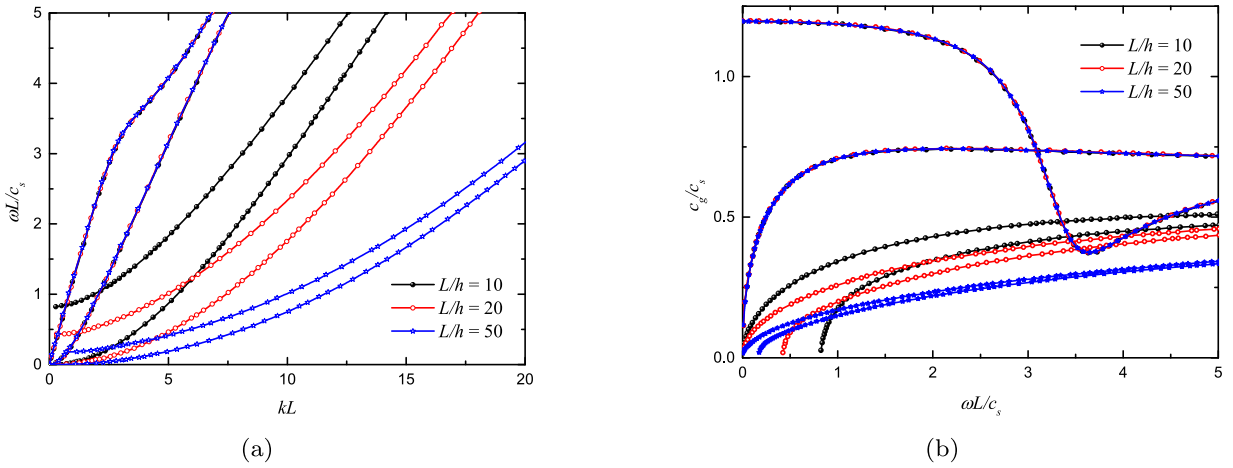

Fig. 11. Influence of the wide-to-thickness ratio of the GPLs on dispersive properties in the piezoelectric composite plates with $f_{GPL} = 0.1\%, N_L = 40$ for Pattern X. (a) Frequency spectra; (b) Group velocity.

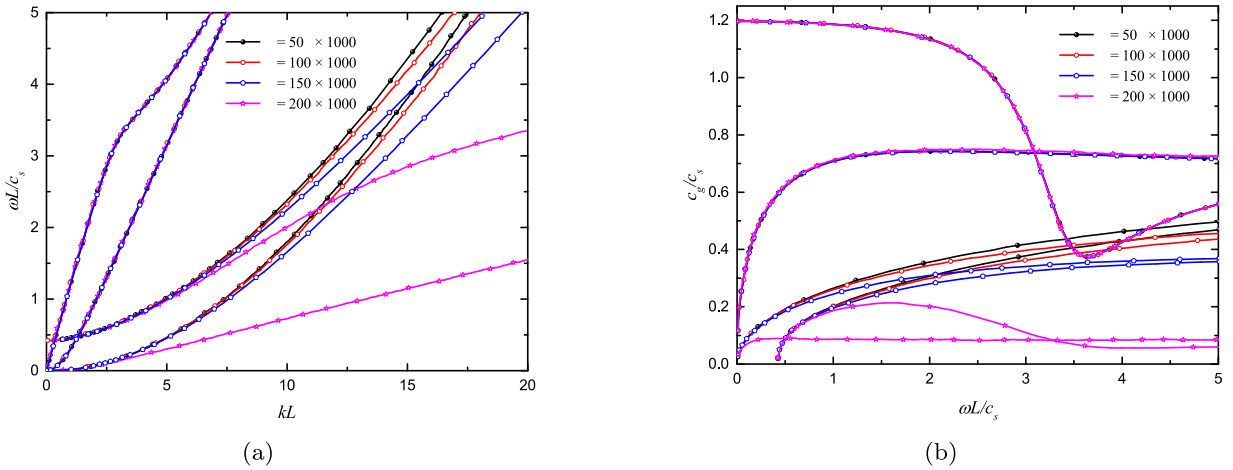

Fig. 12. Influence of the piezoelectric multiple of the GPLs on dispersive properties in the piezoelectric composite plates with $f_{GPL} = 0.1\%, N_L = 40$ for Pattern X. (a) Frequency spectra; (b) Group velocity.

energy. Meanwhile, the larger ratio leads to the delay of cut-off frequency of flexural mode F_2 and it gradually moves to the positive direction.

Besides, the influence of the piezoelectric multiple measuring the piezoelectric effect of the layered GPLs in the composite plate is depicted in Fig. 12. As the piezoelectric multiple grows, the wavenumbers of flexural wave modes become apparently bigger and bigger. Along with the increase of the piezoelectric multiple, the slope of frequency spectra gets lower and the phenomenon is quite obvious in the case of $\alpha = 200 \times 1000$. The group-velocity curves of the flexural modes decrease accordingly but the cutoff frequencies are almost invariant. It is noted clearly that the piezoelectric properties of GPLs have great influence on the flexural wave mode but not on the in-plane modes. Furthermore, the piezoelectric effect of the piezoelectric composite plate reinforced with GPLs is considered by the comparison of dispersion curves with and without piezoelectric constants, as shown in Fig. 13. The piezoelectric effect leads to the reduction of wavenumbers of in-plane modes but that of flexural modes are enhanced. As it describes, the piezoelectric effects can promote the transmission of the in-plane modes and resist the propagation of the flexural modes.

In addition, the size parameter of the GPL is also an important factor influencing dispersive characteristics of wave modes in graphene reinforced piezoelectric composite plate. Fig. 14(a) and (b) indicate that longer or thinner graphene platelets can reduce the wavenumbers of in-plane and flexural wave modes and the energy transmits more quickly. Meanwhile, the effects of size parameters and distribution patterns of GPLs on wave dispersion are shown in Fig. 14(c) at the dimensionless frequency $\Omega = 3$. It is observed obviously that GPLs can effectively control wave propagation as an ideal nanofiller in piezoelectric polymer composites by regulating the reasonable size parameters.

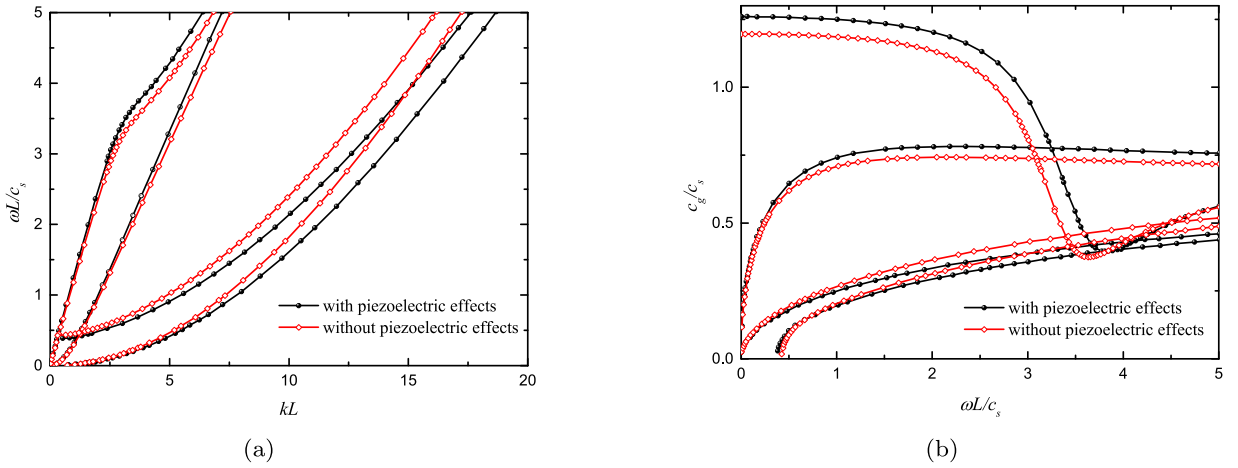

Fig. 13. Piezoelectric effects of the GPLs on dispersive properties in the piezoelectric composite plates with $f_{GPL} = 0.1\%, N_L = 40$ for Pattern X. (a) Frequency spectra; (b) Group velocity.

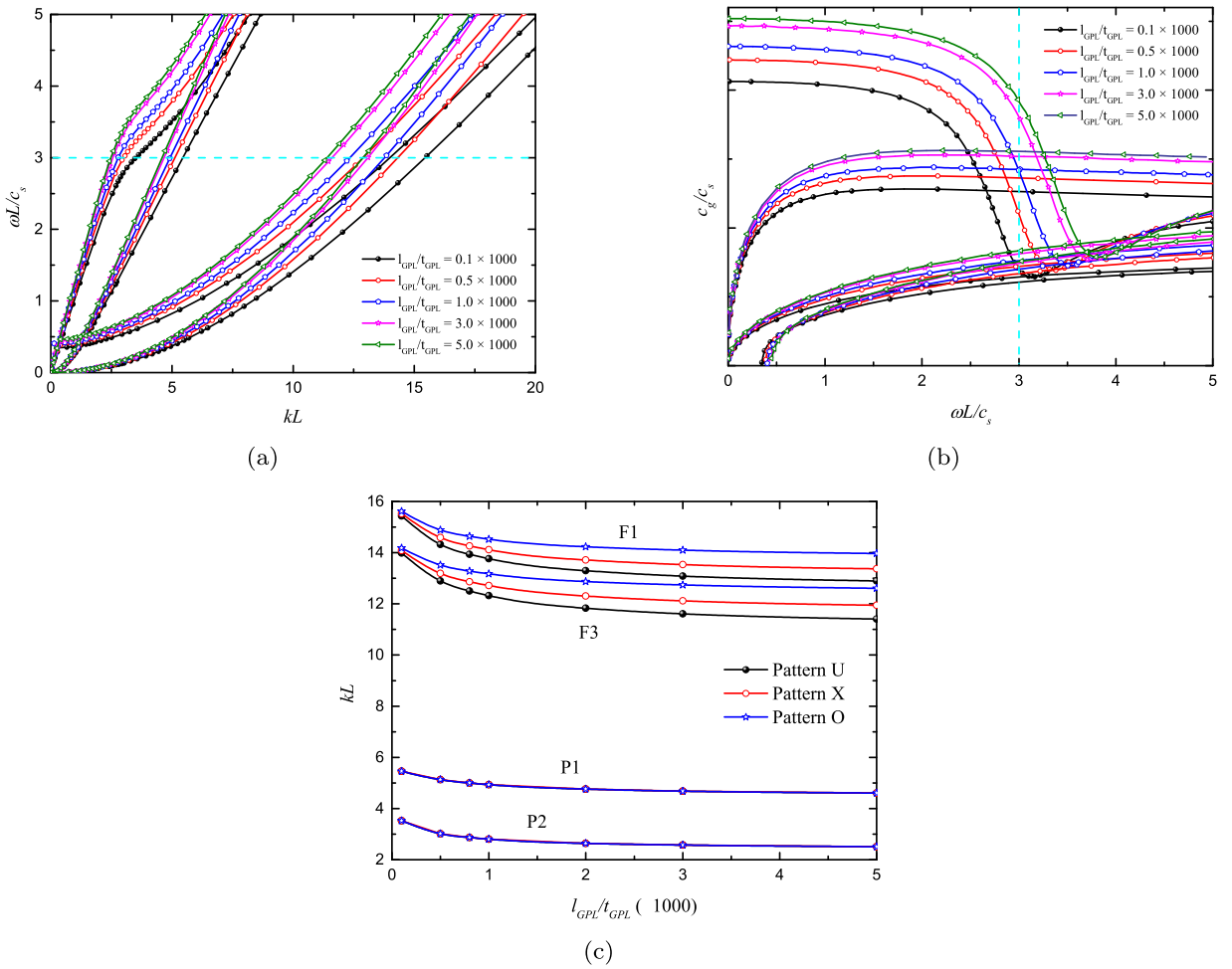

Fig. 14. Effects of size on dispersion curves of the piezoelectric composite plates with $f_{GPL} = 0.1\%, L/h = 20, N_L = 40$ and Pattern U. (a) Frequency spectra; (b) Group velocity; (c) wavenumbers vs size.

5. Conclusions

In this paper, the first order shear deformation theory and isogeometric analysis are employed for the analysis of wave propagation in the piezoelectric composite plate reinforced with GPLs. It is assumed that the GPLs are dispersed following various distribution pattern layer by layer in the thickness direction. A semi-analytical study is performed to systematically investigate the effects of various distribution pattern, volume fraction, size parameters and piezoelectric multiple of GPLs, the effects of piezoelectricity and geometric parameters on dispersion behaviors of elastic waves in functionally graded reinforced piezoelectric composite plate. The results indicate that significant parameters have apparent impact on frequency-spectral and group-velocity curves, and it is noted that the reasonable selections of significant parameters are conductive to efficiently control wave propagation in piezoelectric graphene-polymer composites.

Acknowledgments

The authors wish to acknowledge the support from the Natural Science Foundation of China (grant no. 11972160, 11902117 and 11772130) and the Fundamental Research Funds for the Central Universities, SCUT (grant no. D2192630).

References

[1] C. Bellucci, C. Balasubramanian, F. Micciulla, G. Rinaldi, CNT composites for aerospace applications, J. Exp. Nanosci. 2 (2007) 193–206.
[2] H. Adam, Carbon fibre in automotive applications, Mater. Design. 18 (1997) 349–355.
[3] F. Gauvin, M. Robert, Durability study of vinylester/silicate nanocomposites for civil engineering applications, Poly. degrad. Stabil. 121 (2015) 359–368.
[4] I.M. Daniel, O. Ishai, Engineering Mechanics of Composite Materials, 3, Oxford University Press, New York, 1994.
[5] A.A. Balandin, S. Ghosh, W. Bao, I. Calizo, D. Teweldebrhan, F. Miao, C.N. Lau, Superior thermal conductivity of single-layer graphene, Nano Lett. 8 (2008) 902–907.
[6] K.S. Novoselov, A.K. Geim, S.V. Morozov, D. Jiang, Y. Zhang, S.V. Dubonos, I.V. Grigorieva, A.A. Firsov, Electric field effect in atomically thin carbon films, Science 306 (2004) 666–669.
[7] A. Nieto, A. Bisht, D. Lahiri, C. Zhang, A. Agarwal, Graphene reinforced metal and ceramic matrix composites: a review, Int. Mater. Rev. 62 (2017) 241–302.
[8] X. Huang, X. Qi, F. Boey, H. Zhang, Graphene-based composites, Chem. Soc. Rev. 41 (2012) 666–686.
[9] S. Stankovich, D.A. Dikin, G.H.B. Dommett, K.M. Kohlhaas, E.J. Zimney, E.A. Stach, R.D. Piner, S.T. Nguyen, R.S. Ruoff, Graphene-based composite materials, Nature 442 (1990) 282.
[10] T. Ramanathan, A.A. Abdala, S. Stankovich, D.A. Dikin, A.M. Herrera, R.D. Piner, D.H. Adamson, H.C. Schniepp, X. Chen, R.S. Ruoff, Functionalized graphene sheets for polymer nanocomposites, Nat. Nanotechnol. 3 (2008) 327.
[11] M. Song, S. Kitipornchai, J. Yang, Free and forced vibrations of functionally graded polymer composite plates reinforced with graphene nanoplatelets, Compos. Struct. 159 (2017) 579–588.
[12] J. Yang, D. Chen, S. Kitipornchai, Buckling and free vibration analyses of functionally graded graphene reinforced porous nanocomposite plates based on Chebyshev–Ritz method, Compos. Struct. 193 (2018) 281–294.
[13] Y.H. Dong, B. Zhu, Y. Wang, Y.H. Li, J. Yang, Nonlinear free vibration of graded graphene reinforced cylindrical shells: Effects of spinning motion and axial load, J. Sound. Vib. 437 (2018) 79–96.
[14] Y.H. Dong, B. Zhu, Y. Wang, L.W. He, Y.H. Li, J. Yang, Analytical prediction of the impact response of graphene reinforced spinning cylindrical shells under axial and thermal loads, Appl. Math. Model 71 (2019) 331–348.
[15] Q. Wang, Wave propagation in a piezoelectric coupled cylindrical membrane, Shell, Int. J. Solids Struct. 38 (2001) 8207–8218.
[16] Q. Wang, K. Liew, Analysis of wave propagation in piezoelectric coupled cylinder affected by transverse shear and rotary inertia, Int. J. Solids Struct. 40 (2003) 6653–6667.
[17] K. Dong, X. Wang, Wave propagation characteristics in piezoelectric cylindrical laminated shells under large deformation, Compos. Struct. 77 (2007) 171–181.
[18] J.G. Yu, B. Wu, G.Q. Chen, Wave characteristics in functionally graded piezoelectric hollow cylinders, Arch. Appl. Mech. 79 (2009) 807–824.
[19] H.K. Bisheh, N. Wu, Wave propagation characteristics in a piezoelectric coupled laminated composite cylindrical shell by considering transverse shear effects and rotary inertia, Compos. Struct. 191 (2018) 123–144.
[20] H.K. Bisheh, N. Wu, Analysis of wave propagation characteristics in piezoelectric cylindrical composite shells reinforced with carbon nanotubes, Int. J. Mech. Sci. 145 (2018) 200–220.
[21] M.A. Rafiee, J. Rafiee, Z. Wang, H. Song, Z.Z. Yu, N. Koratkar, Enhanced mechanical properties of nanocomposites at low graphene content, ACS nano 3 (2009) 3884–3890.
[22] R.K. Layek, S. Samanta, D.P. Chatterjee, A.K. Nandi, Physical and mechanical properties of poly (methyl methacrylate)-functionalized graphene/poly (vinylidine fluoride) nanocomposites: Piezoelectric β polymorph formation, Polymer 51 (2010) 5846–5856.
[23] N. Maity, A. Mandal, A.K. Nandi, Hierarchical nanostructured polyaniline functionalized graphene/poly (vinylidene fluoride) composites for improved dielectric performances, Polymer 103 (2016) 83–97.
[24] J.J. Mao, W. Zhang, Linear and nonlinear free and forced vibrations of graphene reinforced piezoelectric composite plate under external voltage excitation, Compos. Struct. 203 (2018) 551–565.
[25] J.J. Mao, W. Zhang, Buckling and post-buckling analyses of functionally graded graphene reinforced piezoelectric plate subjected to electric potential and axial forces, Compos. Struct. 216 (2019) 392–405.
[26] J.N. Reddy, Mechanics of Laminated Composite Plates and Shells: Theory and Analysis, CRC press, 2004.
[27] I. Bartoli, A. Marzani, F.L.D. Scalea, E. Viola, Modeling wave propagation in damped waveguides of arbitrary cross-section, J. Sound. Vib. 295 (2006) 685–707.
[28] C.L. Li, Q. Han, Y.J. Liu, X.C. Liu, B. Wu, Investigation of wave propagation in double cylindrical rods considering the effect of prestress, J. Sound. Vib. 353 (2015) 164–180.
[29] A. Gunawan, S. Hirose, Boundary element analysis of guided waves in a bar with an arbitrary cross-section, Eng. Anal. Bound Elem. 29 (2005) 913–924.
[30] Y.J. Liu, Q. Han, C.L. Li, H.W. Huang, Numerical investigation of dispersion relations for helical waveguides using the scaled boundary finite element method, J. Sound Vib. 333 (2014) 1991–2002.
[31] T.J. Hughes, J.A. Cottrell, Y. Bazilevs, Isogeometric analysis: cad, finite elements, nurbs, exact geometry and mesh refinement, Comput. Method Appl. M. 194 (2005) 4135–4195.
[32] G. Xu, B. Mourrain, R. Duvigneau, A. Galligo, Analysis-suitable volume parameterization of multi-block computational domain in isogeometric applications, Comput. Aided Design 45 (2013) 395–404.
[33] S. Shojaee, N. Valizadeh, E. Izadpanah, T. Bui, T.V. Vu, Free vibration and buckling analysis of laminated composite plates using the NURBS-based isogeometric finite element method, Compos. Struct. 94 (2012) 1677–1693.

[34] N. Valizadeh, S. Natarajan, O.A. Gonzalez-Estrada, T. Rabczuk, T.Q. Bui, S.P.A. Bordas, NURBS-based finite element analysis of functionally graded plates: static bending, vibration, buckling and flutter, Compos. Struct. 99 (2013) 309–326.
[35] S.H. Yin, J.S. Hale, T.T. Yu, T.Q. Bui, S.P.A. Bordas, Isogeometric locking-free plate element: a simple first order shear deformation theory for functionally graded plates, Compos. Struct. 118 (2014) 121–138.
[36] T.T. Yu, S.H. Yu, T.Q. Bui, S. Hirose, A simple FSDT-based isogeometric analysis for geometrically nonlinear analysis of functionally graded plates, Finite Elem. Anal. Des. 96 (2015) 1–10.
[37] T.T. Yu, S.H. Yin, T.Q. Bui, S.F. Xia, S. Tanaka, S. Hirose, NURBS-based isogeometric analysis of buckling and free vibration problems for laminated composites plates with complicated cutouts using a new simple FSDT theory and level set method, Thin Wall Struct. 101 (2016) 141–156.
[38] T.V. Vu, N.H. Nguyen, A. Khosravifard, M.R. Hematiyan, S. Tanaka, T.Q. Bui, A simple FSDT-based meshfree method for analysis of functionally graded plates, Eng. Anal. Bound. Elem. 79 (2017) 1–12.
[39] C.H. Thai, A.J.M. Ferreira, T.D. Tran, V.P. Phung, Free vibration, buckling and bending analyses of multilayer functionally graded graphene nanoplatelets reinforced composite plates using the NURBS formulation, Compos. Struct. 220 (2019) 749–759.
[40] N. Nguyen-Thanh, K. Zhou, X. Zhuang, P. Areias, H. Nguyen-Xuan, Y. Bazilevs, T. Rabczuk, Isogeometric analysis of large-deformation thin shells using RHT-splines for multiple-patch coupling, Comput. Method Appl. M. 316 (2017) 1157–1178.
[41] B. Vu-Bac, T.X. Duong, T. Lahmer, X. Zhuang, R.A. Sauer, H.S. Park, T. Rabczuk, A NURBS-based inverse analysis for reconstruction of nonlinear deformations of thin shell structures, Comput. Method Appl. M. 331 (2018) 427–455.
[42] H. Ghasemi, H.S. Park, T. Rabczuk, A level-set based IGA formulation for topology optimization of flexoelectric materials, Comput. Method Appl. M. 313 (2017) 239–258.
[43] H. Ghasemi, H.S. Park, T. Rabczuk, A multi-material level set-based topology optimization of flexoelectric composites, Comput. Method Appl. M. 332 (2018) 47–62.
[44] B.H. Nguyen, S.S. Nanthakumar, Z. X, P. Wriggers, J. X, T. Rabczuk, Dynamic flexoelectric effect on piezoelectric nanostructures, Eur. J. Mech. A-Solid 71 (2018) 404–409.
[45] J. Mitchell, J. Reddy, A refined hybrid plate theory for composite laminates with piezoelectric laminae, Int. J. Solids Struct. 32 (1995) 2345–2367.
[46] M. Shokrieh, S. Ghoreishi, M. Esmkhani, Toughening mechanisms of nanoparticle-reinforced polymers, in: Toughening Mechanisms in Composite Materials, Elsevier, 2015, pp. 295–320.
[47] N. Maity, A. Mandal, A.K. Nandi, Hierarchical nanostructured polyaniline functionalized graphene/poly (vinylidene fluoride) composites for improved dielectric performances, Polymer 103 (2016) 83–97.
[48] K. Xu, K. Wang, W. Zhao, W.Z. Bao, et al., The positive piezoconductive effect in graphene, Nat. commun. 6 (2015) 8119.
[49] L. Piegl, W. Tiller, The NURBS Book, Springer Science, 2012.
[50] H.S. Shen, C.L. Zhang, Thermal buckling and postbuckling behavior of functionally graded carbon nanotube-reinforced composite plates, Mater. Design 31 (2010) 3403–3411.
[51] J. Zhu, J. Yang, S. Kitipornchai, Dispersion spectrum in a functionally graded carbon nanotube-reinforced plate based on first-order shear deformation plate theory, Compos. B Eng. 53 (2013) 274–283.